Radiative transition decay width of $\psi_2(3823) \to \gamma\chi_{c1}$ from lattice QCD

Ning Li,[1,*] Yan Gao,[1] Feiyu Chen,[2,3] Ying Chen,[2,3] Xiangyu Jiang,[2,3] Chunjiang Shi,[2,3] and Wei Sun[2]

[1]School of Sciences, Xi'an Technological University, Xi'an 710021, People's Republic of China
[2]Institute of High Energy Physics, Chinese Academy of Sciences, Beijing 100049, People's Republic of China
[3]School of Physical Sciences, University of Chinese Academy of Sciences, Beijing 100049, People's Republic of China

(Received 30 September 2023; accepted 8 January 2024; published 31 January 2024)

We present an exploratory $N_f = 2$ lattice QCD study of $\psi_2(3823) \to \gamma\chi_{c1}$ at a pion mass $m_\pi \approx 350$ MeV. The related two-point and three-point functions are calculated using the distillation method. The electromagnetic multipole form factor $\hat{V}(0) = 2.083(11)$ for $J/\psi \to \gamma\eta_c$ is consistent with previous lattice results. The form factors $\hat{E}_1(0)$, $\hat{M}_2(0)$, and $\hat{E}_3(0)$ for $\Gamma(\chi_{c2} \to \gamma J/\psi)$ have the same hierarchy as that derived from experiments, and the predicted decay width $\Gamma(\chi_{c2} \to \gamma J/\psi) = 368(5)$ keV is in excellent agreement with the Particle Data Group value 374(10) keV and previous lattice QCD results in the quenched approximation. The same strategy is applied to the study of the process $\psi_2(3823) \to \gamma\chi_{c1}$, and the partial decay width is predicted to be 337(27) keV. According to the BESIII constraints on the $\psi_2(3823)$ decay channels and some phenomenological results, we estimate the total width $\Gamma(\psi_2(3823)) = 520(100)$ keV.

DOI: 10.1103/PhysRevD.109.014513

I. INTRODUCTION

Charmonium states are usually thought of as the bound states of charm quark and antiquark ($c\bar{c}$) in the conventional quark model. Since the charm quark is relatively heavy, a nonrelativistic description of the internal structure of charmonium is acceptable to some extent, especially for the low-lying states. In the nonrelativistic potential model, a charmonium state can be assigned to a $n^{2S+1}L_J$ state, where n, S, and L are the radial quantum number, the total spin of the $c\bar{c}$ pair, and the orbital angular momentum, respectively. Consequently, it gives the J^{PC} quantum number of the state. For $n = 1$, the S-wave charmonium (J/ψ and η_c) and the P-wave charmonium (h_c and $\chi_{c0,1,2}$) have been well established, but the D-wave supermultiplet (1^1D_2, $1^3D_{1,2,3}$) is not complete yet. Experimentally, apart from the vector charmonium $\psi(3770)$ that is assigned to be (predominantly) the 1^3D_1 state, other $1D$ charmonium have escaped from the experimental search for a long time. In 2013, the Belle Collaboration reported the first evidence for a 2^{--} charmoniumlike state $X(3823)$ of a mass $3823.1 \pm 1.8 \pm 0.7$ MeV in the $\chi_{c1}\gamma$ invariant mass spectrum of the decay processes $B \to \chi_{c1}\gamma K$ [1]. In 2015, the BESIII Collaboration also observed $X(3823)$ in the $\gamma\chi_{c1}$ system with a statistical significance of 6.2σ in the process $e^+e^- \to \pi^+\pi^-\chi_{c1}\gamma$ [2]. The mass of $X(3823)$ is measured to be $3823.7 \pm 1.3 \pm 0.7$ MeV, which is consistent with that measured by Belle and confirms the existence of $X(3823)$. The properties of $X(3823)$, such as its mass and decay modes $\chi_{c1,2}\gamma$ [3], are consistent with the theoretical expectations for those of the $1D$ state 1^3D_2. Now $X(3823)$ is named by $\psi_2(3823)$ in Particle Data Group (PDG) [4]. The observation of $\psi_2(3823)$ in the process $e^+e^- \to \pi^0\pi^0\psi_2(3823)$ by BESIII [3,5] provides a further support of its quantum number $J^{PC} = 2^{--}$. Recently, the LHCb Collaboration observed a new charmonium state $X(3842)$ near the $D\bar{D}$ threshold using proton-proton collision data [6]. Its mass $m_{X(3842)} = 3842.72 \pm 0.16 \pm 0.12$ MeV and the very small width $\Gamma_{X(3842)} = 2.79 \pm 0.51 \pm 0.35$ MeV suggest $X(3842)$ to be a candidate for the 1^3D_3 charmonium state (named as ψ_3 in PDG). Thus, the $1D$ spin triplet is in space, while the spin singlet $1D$ state η_{c2} is still missing.

The width of $\psi_2(3823)$ is expected to be very small since it lies a little higher than the $D\bar{D}$ threshold but lower than $D\bar{D}^*$ and $D^*\bar{D}^*$ threshold. However, $\psi_2(3823)$ cannot decay into $D\bar{D}$ whose permitted quantum numbers are $J^{PC} = (\text{even})^{++}$ and $(\text{odd})^{--}$. Thus, its major decay modes should be radiative and hadronic transitions into other charmonium states. Phenomenological studies predict the partial widths $\Gamma(\psi_2 \to \gamma\chi_{c1}) \sim 200$–$300$ keV, $\Gamma(\psi_2 \to \gamma\chi_{c2}) \sim 60$ keV [7,8], and $\Gamma(\psi_2 \to J/\psi\pi\pi) \sim 160$ keV [9]. (However, BESIII gives the upper limits $\Gamma(\psi_2(3823) \to \pi^+\pi^- J/\psi)/\Gamma(\psi_2(3823) \to \gamma\chi_{c1}) < 0.06$ and $\Gamma(\psi_2(3823) \to \pi^0\pi^0 J/\psi)/\Gamma(\psi_2(3823) \to \gamma\chi_{c1}) < 0.11$, which are in striking

*lining@xatu.edu.cn

contrast to the theoretical expectation.) This indicates $\psi_2 \to \gamma\chi_{c1}$ might be the most important decay channel. Experimentally, LHCb gives an upper bound $\Gamma_{\psi_2} < 5.2$ MeV [10], while a recent BESIII measurement decreases this limit to be $\Gamma_{\psi_2} < 2.9$ MeV at the 90% confidence level [11]. So reliable determination of the partial width $\psi_2(3823) \to \gamma\chi_{c1}$ is very helpful to estimate the total width of $\psi_2(3823)$.

A first-principle calculation of $\psi_2(3823)$ decays is desired two fold. First, charmonium states are located at the intermediate energy scale of QCD, where both perturbative and nonperturbative physics are present, and charmonium states are considered as an ideal test ground for quantum chromodynamics (QCD). Second, the comparison of the quark model predictions and the first-principle calculation can indicate to what extent the quark model describes the properties of charmonium. The numerical lattice QCD calculation is known as an *ab initio* approach to solve the low energy problems of QCD and has been extensively applied to the study of radiative transition between various charmonium [12–28].

In this simulation, we calculate the radiative transition decay width of $\psi_2 \to \chi_{c1}\gamma$ in the framework of $N_f = 2$ lattice QCD. We compute related two-point and three-point correlation functions by the implementation of the distillation method [27,29,30]. This smearing technique helps us use optimized operators of definite momentum at both source and sink as well as insert a vector current operator of definite momentum. Therefore, it has efficiently decreased the errors of physical quantities extracted from the correlation functions. As a calibration of possible systematic uncertainties with our lattice setup, we also calculate the radiative transition decay width of $J/\psi \to \eta_c\gamma$ and $\chi_{c2} \to J/\psi\gamma$ and compare them with previous lattice results and experimental values.

This paper is organized as follows. Section II introduces the strategies for computing the form factors for radiative decays. In Sec. III, we explain the numerical details such as the gauge ensembles and the calculation of two-point and three-point functions using the distillation method. Section IV presents the lattice results of the transition processes $J/\psi \to \eta_c\gamma, \chi_{c2} \to J/\psi\gamma$ and $\psi_2 \to \chi_{c1}\gamma$, as well as the related discussions. Section V is the summary of this work.

II. FORMALISM

For a radiative transition process $i(p_i) \to \gamma f(p_f)$, the partial decay width can be expressed in terms of the electromagnetic multipole form factors $F_k(Q^2)$ at $Q^2 = 0$, namely,

$$\Gamma(i \to f\gamma) = \frac{1}{2J_i + 1}\alpha\frac{|\mathbf{q}|}{m_i^2}\sum_k |F_k(0)|^2, \tag{1}$$

where $\alpha = 1/137$ is the fine structure constant at the charm quark scale; $\mathbf{q}$ is the momentum of the photon in the final state with $|\mathbf{q}| = \frac{(m_i^2 - m_f^2)}{2m_i}$ and $Q^2 = -q^2 = (p_i - p_f)^2$. The multipole form factors $F_k(Q^2)$ are encoded in the matrix element of the electromagnetic current $J_\mu^{\mathrm{em}}(0)$ between the initial and final hadron states, namely,

$$\begin{aligned}&\langle f, p_f, r_f|J_\mu^{\mathrm{em}}(0)|i, p_i, r_i\rangle \\ &\equiv \sum_k \alpha_\mu^k(p_i, p_f, \epsilon^{(r_f),*}, \epsilon^{(r_i)})F_k(Q^2),\end{aligned} \tag{2}$$

where $\epsilon^{(r)}$ refers to the polarization vectors (tensors) of the initial and the final hadron states; α_k are known functions of $p_i, p_f, \epsilon^{(r_{i,f})}$ that are determined through the multipole decomposition [12,14,16].

The matrix element on the left-hand side can be extracted from the following three-point correlation functions with an insertion of the local current $J_\mu^{\mathrm{em}}(x)$, i.e.,

$$\begin{aligned}G_{f\mu i}(t_f, t; \mathbf{p}_f, \mathbf{p}_i) = &\sum_{\mathbf{x},\mathbf{y}} e^{-i\mathbf{p}_f\cdot\mathbf{x}}e^{i\mathbf{q}\cdot\mathbf{y}} \\ &\times \langle\Omega|T\mathcal{O}_f(t_f, \mathbf{x})J_\mu^{\mathrm{em}}(t, \mathbf{y}) \\ &\times \mathcal{O}_i^\dagger(0, \mathbf{0})|\Omega\rangle,\end{aligned} \tag{3}$$

where $\mathcal{O}_f(t_f, \mathbf{x})$ and $\mathcal{O}_i^\dagger(0, \mathbf{0})$ are interpolating operators for the final and the initial hadron states, respectively, $\mathbf{q} = \mathbf{p}_i - \mathbf{p}_f$ is the momentum of the (virtual) photon, and J_μ^{em} is the electromagnetic vector current whose explicit form is

$$\begin{aligned}J_\mu^{\mathrm{em}}(x) &= \sum_q Q_q\overline{\psi_q}(x)\gamma_\mu\psi_q(x) \\ &\to \frac{2e}{3}\overline{c}(x)\gamma_\mu c(x) \\ &= \frac{2e}{3}J_\mu,\end{aligned} \tag{4}$$

with q referring to u, d, s, c, b quark flavors. For charmonium radiative decays, since u, d, s, b quarks contribute to $G_{f\mu i}(t_2, t; \mathbf{p_2}, \mathbf{p_1})$ through disconnected quark diagrams, which are suppressed by OZI rules, we only consider the electromagnetic current of charm quark with $Q_c = 2e/3$ in the practical calculation.

After inserting a complete set of states between the electromagnetic vector current and the interpolating operators, Eq. (3) has the following asymptotic form in the $t_f \gg t \gg 1$ limit,

$$\begin{aligned}G_{f\mu i}(t_f, t; \mathbf{p}_f, \mathbf{p}_i) \overset{t_f \gg t \gg 1}{\longrightarrow} &\frac{e^{-E_f t_f}e^{-(E_i - E_f)t}}{4E_i(\mathbf{p}_i)E_f(\mathbf{p}_f)} \\ &\times \langle\Omega|\mathcal{O}_f|f(\mathbf{p}_f)\rangle\langle i(\mathbf{p}_i)|\mathcal{O}_i^\dagger|\Omega\rangle \\ &\times \langle f(\mathbf{p}_f)|J_\mu^{\mathrm{em}}(0)|i(\mathbf{p}_i)\rangle.\end{aligned} \tag{5}$$

TABLE I. Parameters of the gauge ensemble.

$L^3 \times T$	β	a_t^{-1} (GeV)	ξ	m_π (MeV)	$N_{\rm cfg}$
$16^3 \times 128$	2.0	6.894(51)	∼5.3	348.5(1.0)	689

In order to extract the matrix element $\langle f|J_\mu^{\rm em}(0)|i\rangle$, we need to the energies and spectral weight of the final and the initial states, i.e., E_i, E_f, $\langle\Omega|\mathcal{O}_f|f(\mathbf{p}_f)\rangle$, and $\langle i(\mathbf{p}_i)|\mathcal{O}_i^\dagger|\Omega\rangle$. They can be determined from the two-point correlation function,

$$\begin{aligned} C(t,\mathbf{p}) &= \sum_{\mathbf{x}} e^{-i\mathbf{p}\cdot\mathbf{x}}\langle\Omega|\mathcal{O}(t,\mathbf{x})\mathcal{O}^\dagger(0,\mathbf{0})|\Omega\rangle \\ &= \sum_n \frac{|\langle\Omega|\mathcal{O}(0)|n,\mathbf{p}\rangle|^2}{2E_n(\mathbf{p})} e^{-E_n(\mathbf{p})t} \\ &\to \frac{|Z(\mathbf{p})|^2}{2E(\mathbf{p})} e^{-E(\mathbf{p})t} (t\to\infty), \end{aligned} \tag{6}$$

where $E(\mathbf{p})$ is the energy of the ground state $|1,\mathbf{p}\rangle$, and $Z(\mathbf{p}) = \langle\Omega|\mathcal{O}(0)|1,\mathbf{p}\rangle$ is defined. So the key problem in this work is to calculate the two-point and three-point functions, from which the transition amplitude can be derived. It should be notified that the polarizations of $J \neq 0$ particles are not spelled out explicitly in the discussion above for simplicity, but are taken into account the in the concrete calculations.

III. SIMULATION DETAILS

We use a subset of the $N_f = 2$ gauge ensemble generated on an $L^3 \times T = 16^3 \times 128$ anisotropic lattice with the anisotropy parameter $\xi = a_s/a_t = 5.3$ (a_s and a_t are the spatial and temporal lattice spacings, respectively) [31]. The sea quark mass is tuned to give the pion mass $m_\pi \approx 350$ MeV. The parameters of the gauge ensemble are listed in Table I. For the valence charm quark, we adopt the clover fermion action in Refs. [32–34], and the charm quark mass parameter is set by $(m_{\eta_c} + 3m_{J/\psi})/4 = 3069$ MeV. For each source time slice $\tau \in [0, T-1]$ on each gauge configuration, the perambulators of charm quark are calculated in the Laplacian Heaviside (LH) subspace spanned by $N_{\rm vec} = 50$ eigenvectors with lowest eigenvalues.

A. Charmonium spectrum

In this section, we introduce briefly the distillation method to compute two-point correlation function [29]. The distillation method provides automatically the Laplacian Heaviside (LH) smearing scheme for quark fields. The LH smeared charm quark field on each time slice t is defined as

$$c^{(s)}(\mathbf{x},t) = \sum_{\mathbf{y}} \square_{\mathbf{x},\mathbf{y}}(t) c(\mathbf{y},t), \tag{7}$$

with the smearing function $\square_{\mathbf{x},\mathbf{y}}(t)$ being defined by the eigenvectors $\{\xi_{\mathbf{x}}^{(n)}(t), n = 1,2,\ldots,N_{\rm vec}\}$ that span the LH subspace, namely,

$$\square_{\mathbf{xy}}(t) = \sum_{n=1}^{N} \xi_{\mathbf{x}}^{(n)}(t)\xi_{\mathbf{y}}^{(n)\dagger}(t). \tag{8}$$

Subsequently, each interpolation operator $\mathcal{O}$ in Eqs. (3) and (6) is built in terms of $c^{(s)}$

$$\mathcal{O}(t,\mathbf{x}) = \sum_{\mathbf{y}} \bar{c}^{(s)}(t,\mathbf{x})\Gamma(\mathbf{x},\mathbf{y};t)c^{(s)}(t,\mathbf{x}), \tag{9}$$

where $\Gamma(\mathbf{x},\mathbf{y};t)$ is a specific combination of γ matrices and the discretized covariant derivatives and dictates the quantum number of the operators. (The Γ's for the charmonium states involved in this work are listed in Table II.) A normal Fourier transformation can project out the operator that annihilates a charmonium state with a definite spatial momentum $\mathbf{p}$,

$$\begin{aligned} \mathcal{O}(t,\mathbf{p}) &= \sum_{\mathbf{y}} e^{-i\mathbf{p}\cdot\mathbf{y}}\mathcal{O}(t,\mathbf{x}) \\ &\equiv [\bar{c}_{\mathbf{x}}\square_{\mathbf{xy}}e^{-i\mathbf{p}\cdot\mathbf{y}}\Gamma_{\mathbf{yz}}\square_{\mathbf{zw}}c_{\mathbf{w}}](t) \\ &\equiv [\bar{c}\square\Gamma(\mathbf{p})\square c](t), \end{aligned} \tag{10}$$

where the subscripts $\mathbf{x},\mathbf{y},\mathbf{z},\mathbf{w}$ in the second row mean that the spatial coordinates are viewed as matrix indices with the duplicated subscripts being summed implicitly, and $\Gamma(t,\mathbf{p})$ in the third row is $[\Gamma(p)]_{\mathbf{xy}}(t) = e^{-i\mathbf{p}\cdot\mathbf{x}}\Gamma_{\mathbf{xy}}(t)$. The two-point correlation function can be expressed as

TABLE II. The interpolating operators [36] and masses of charmonium states involved in this work. The PDG masses values [4] of these states are also presented for comparison.

Meson	η_c	J/ψ	χ_{c1}	χ_{c2}	ψ_2
Γ	γ_5	γ_i	$\gamma_i\gamma_5$	$\lvert\epsilon_{ijk}\rvert\gamma_j\nabla_k(\mathcal{Q}_{ijk}\gamma_j\nabla_k)$	$\lvert\epsilon_{ijk}\rvert\gamma_5\gamma_j\nabla_k(\mathcal{Q}_{ijk}\gamma_5\gamma_j\nabla_k)$
m (MeV)	2976.8(0.4)	3099.9(0.4)	3563.1(1.6)	3610.8(1.7)	3907.5(7.6)
m (MeV) (PDG) [4]	2983.9(0.4)	3096.900(0.006)	3510.67(0.05)	3556.17(0.07)	3823.7(0.5)

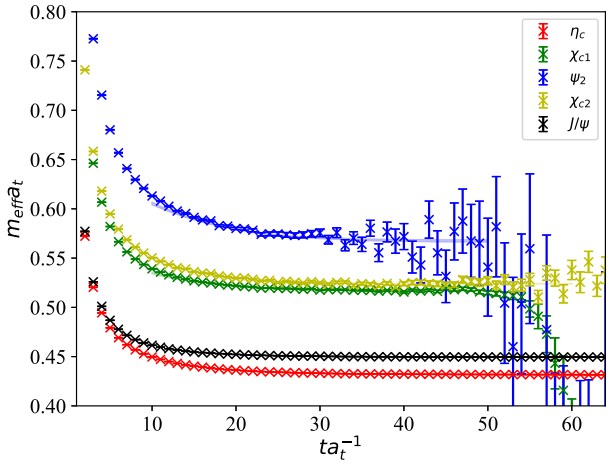

FIG. 1. Charmonium effective mass plateaus. From lower to higher values, the plateau corresponds to the charmonium state η_c, J/ψ, χ_{c1}, χ_{c2}, ψ_2, respectively.

$$C(t,\mathbf{p}) = \langle\Omega|[\bar{c}\Box\Gamma(\mathbf{p})\Box c](t)[\bar{c}\Box\Gamma(\mathbf{p})\Box c](0)|\Omega\rangle = \tau_{nm}(0,t)\Phi^{\Gamma}_{mp}(t,\mathbf{p})\tau_{pq}(t,0)\Phi^{\Gamma}_{qn}(0,\mathbf{p}), \quad (11)$$

where $\tau_{pq}(t,0) = \xi^{\dagger}_p(t)M^{-1}(t,0)\xi_q(0)$ is the perambulators that are obtained by inverting the Dirac matrix M on sources $\xi_q(0)\{q = 1,\ldots,N_{\text{vec}}\}$. $\Phi^{\Gamma}_{mp}(t,\mathbf{p}) = [\xi^{\dagger}_m\Gamma(\mathbf{p})\xi_p](t)$ is the elemental that reflects the structure of the corresponding operator. In this study, we calculate the spectrum of charmonium states η_c, J/ψ, χ_{c1}, χ_{c2}, ψ_2). The mass values for these meson are listed in Table II, where also listed are the Γ operators in Eq. (9) for the charmonium states involved in this work. Figure 1 shows the effective mass functions $m_{\text{eff}}a_t = \ln\frac{C(t,\mathbf{0})}{C(t+a_t,\mathbf{0})}$ of the correlation functions of these charmonium states. In the calculation of charmonium two-point functions, we do not include the contribution from the disconnected diagrams, which are expected to be negligible. (This is also supported to some extent by a recent lattice QCD study [35]).

B. Three-point functions

Since the operators $\mathcal{O}_{i,f}$ are constructed in terms of the LH smeared quark fields [see Eq. (9)], the Wick's contraction of the three-point correlation function in Eq. (3) results in the explicit expression for a given t_f,

$$\begin{aligned} &G_{f\mu i}(t_f,t;\mathbf{p}_f,\mathbf{p}_i) \\ &\to \langle\Omega|[\bar{c}\Box\Gamma^f(\mathbf{p}_f)\Box c](t_f)J_\mu(t)[\bar{c}\Box\Gamma^i(\mathbf{p}_i)\Box c(0)]|\Omega\rangle \\ &= \langle\Omega|[\bar{c}\Box\Gamma^f(\mathbf{p}_f)\Box c](t_f)[\bar{c}\gamma_\mu c](t)[\bar{c}\Box\Gamma^i(\mathbf{p}_i)\Box c](0)|\Omega\rangle \\ &= \tau_{nm}(0,t_f)\Phi^{\Gamma^f}_{mp}(t_f,\mathbf{p}_f)\mathcal{G}_{pq\mu}(t_f,t,0)\Phi^{\Gamma^i}_{qn}(0,\mathbf{p}_i), \end{aligned} \quad (12)$$

where $\mathcal{G}_{pq\mu}(t_f,t,0) = \xi^{\dagger}_p(t_f)M^{-1}(t_f,t)\Gamma_\mu M^{-1}(t,0)\xi_q(0)$ is called generalized perambulator. The schematic diagram

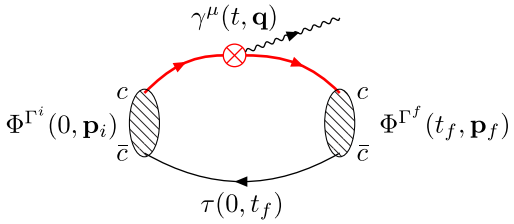

FIG. 2. The schematic diagram of the calculation three-point function using the distillation method. The filled black line is the perambulator $\tau(0,t_f)$ of the charm quark. The red line with the vector current insertion is the generalized perambulator $\mathcal{G}_{pq\mu}(t_f,t,0)$ in Eq. (12). The hatched ellipses indicates the wave functions $\Phi^{i,f}$ of the initial and final charmonia.

for the calculation of $G_{f\mu i}(t)$ is shown in Fig. 2, where the hatched ellipses stand for the wave functions $\Phi^{i,f}$ of the initial and final charmonia, and the filled black line is the perambulator $\tau(t_1,t_2)$ of the charm quark, while the red line with the vector current insertion is the generalized perambulator, which are calculated separately owing to the insertion of the local current [30].

To reduce the unknown factors in Eq. (5), the ratio between the three-point function and the two-point function is introduced, i.e.,

$$R_\mu(t,t_f) = \frac{Z_i(\mathbf{p}_i)Z_f(\mathbf{p}_f)G_{f\mu i}(t_f,t;\mathbf{p}_f,\mathbf{p}_i)}{C_f(t_f-t,\mathbf{p}_f)C_i(t,\mathbf{p}_i)} \simeq \frac{\langle f(p_f)|J_\mu(0)|i(p_i)\rangle}{4\sqrt{E_f(p_f)E_i(p_i)}}. \quad (13)$$

Here, the second line is valid when $t_f \gg t \gg 1$ and only the ground state dominates. C_i and C_f are two-point correlation functions of the initial state and the final state, respectively. $G_{f\mu i}(t_f,t;\mathbf{p}_f,\mathbf{p}_i)$ is a three-point correlation function. Since the matrix element $\langle f(p_f)|J_\mu(0)|i(p_i)\rangle$ is independent of t, it can be derived in the plateau region that $R_\mu(t,t_f)$ is independent of t where the ground states of the initial and final state charmonia dominate the contribution.

After the matrix element is obtained at each value of Q^2, we can use the multipole expansion expression Eq. (2) to extract the form factors $F_k(Q^2)$. In order to give a theoretical prediction of the partial decay width using Eq. (1), we need the on-shell form factors $F_k(Q^2=0)$, which can be determined through the interpolation or extrapolation of $F_k(Q^2)$ with respect to Q^2. Usually, one can use the quark model-inspired function forms to do the interpolation or extrapolation (see below), or just use polynomials of Q^2 in the neighborhood of $Q^2 = 0$.

IV. CHARMONIUM RADIATIVE TRANSITIONS

Since we have only one gauge ensemble of a single lattice spacing, a single light quark mass, we first calculate the

partial decay widths $\Gamma(J/\psi \to \gamma\eta_c)$ and $\Gamma(\chi_{c2} \to \gamma J/\psi)$. The comparison of our results with those of previous lattice calculations and experimental values is used as a calibration of the possible systematic uncertainties of our lattice setup. Then, the similar calculation is applied to the process $\psi_2 \to \gamma\chi_{c1}$.

The continuum current form in Eq. (4) is not conserved on the lattice and should be renormalized. We adopt the strategy used in Refs. [12,16] to determine the renormalization factor Z_V. By calculating the relevant electromagnetic form factors of η_c, we obtain $Z_V^t = 1.165(3)$ for the temporal component of $J_\mu^{\rm em}$ and $Z_V^s = 1.118(4)$ for its spatial components [25,26]. In this work, only the spatial components of $J_\mu^{\rm em}$ are involved in the calculation, and the renormalization constant Z_V^s is incorporated implicitly in the current insertion.

As shown in Fig. 2, the current insertion to each quark line gives the same result, so we only consider one of the two insertions. On the other hand, the electric charge $Q_c = 2e/3$ of the charm quark is not included in J_μ in the practical calculation for simplicity; therefore, the form factors $\hat{F}_k(Q^2)$ extracted from three-point functions is related to the original ones $F_k(Q^2)$ in Eq. (2) by the convention

$$F_k(Q^2) = 2 \times \frac{2e}{3} \times \hat{F}_k(Q^2). \tag{14}$$

This convention applies to all the form factors considered in this work.

The radiative transitions in this study are all studied in the rest frame of the initial state; namely, the spatial momentum of the initial state is set to be $\mathbf{p}_i = 0$ such that $\mathbf{q} = -\mathbf{p}_f$. The momentum mode $\mathbf{n} = (n_1, n_2, n_3)$ of the final state momentum $\mathbf{p}_f = \frac{2\pi}{La_s}\mathbf{n}$ is represented by (0,0,0), (0,0,1),(0,1,1),(0,0,2),(0,1,2), or (1,1,2), meaning that all the momentum modes that can be obtained by applying the lattice symmetry operation to each mode $\mathbf{n}$ in the list are sorted in the same mode denoted by $\mathbf{n}$. Obviously, for a specific transition process, the $\mathbf{p}_f$'s in each mode give the same $Q^2 = -(E_f - m_i)^2 + \mathbf{p}_f^2$, and the Q^2 of different modes are different from each other.

A. $J/\psi \to \gamma\eta_c$

The transition amplitude for the process for $J/\psi \to \eta_c\gamma$ involves only one form factor $V(Q^2)$ [12,15],

$$\begin{aligned}&\langle \eta_c(\mathbf{p}_f)|J_\mu^{em}|J/\psi(\mathbf{p}_i), r\rangle \\ &= \frac{2V(Q^2)}{m_{\eta_c} + m_{J/\psi}} \epsilon^{\alpha\mu\beta\gamma} p_{f,\mu} p_{i,\beta} \epsilon_\gamma(\mathbf{p}_i, r).\end{aligned} \tag{15}$$

In practice, we derive the transition amplitude using Eq. (13) first and then obtain $\hat{V}(Q^2; t, t_f)$ by solving Eqs. (14) and (15) for each momentum $\mathbf{p}_f$ of the final state. For $t_f = 64a_t$, the t dependence of $\hat{V}(Q^2; t, t_f)$ for different values of Q^2 is shown in Fig. 3, where the obvious t dependence near $t = 0$ and $t = t_f$ is attributed to the contamination from higher initial states and higher final states, respectively. Therefore, we use the following function form:

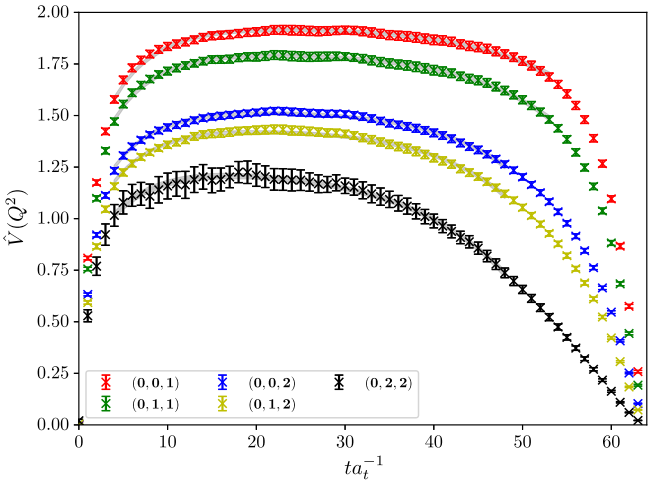

FIG. 3. The t dependence of $\hat{V}(Q^2)$. The momentum of final particle is $\mathbf{p_f} = \frac{2\pi}{\mathbf{a_s L}}(\mathbf{n_x n_y n_z})$; the legend denotes explicit value of (n_x, n_y, n_z). The points are lattice data, and the shaded bands are the fit results using the function form in Eq. (16).

$$\hat{V}(Q^2; t, t_f) = \hat{V}(Q^2)(1 + \delta_1 e^{\Delta_1 t} + \delta_2(Q^2) e^{-\Delta_2(t_f - t)}), \tag{16}$$

to fit the data at different Q^2 simultaneously. Since we set the initial state to be in its rest frame and let the final state move with a specific momentum, the parameters δ_1 and Δ_1 describe the contribution from the higher initial states and are thereby uniform for all the different values of Q^2 involved, while the parameters δ_2 and Δ_2 for the higher final states have Q^2 dependence. The fit results are also illustrated by colored bands in Fig. 3, where one can see the fit form in Eq. (16) describes the data very well. The fitted values of $\hat{V}(Q^2)$ are shown in Table III. In order to obtain the on-shell form factor $\hat{V}(Q^2 = 0)$, which enters the partial decay width as

$$\Gamma(J/\psi \to \gamma\eta_c) = \frac{64}{27}\alpha \frac{|\mathbf{q}|^3}{(m_1 + m_2)^2} |\hat{V}(0)|^2, \tag{17}$$

we perform a Q^2-interpolation using the function form

$$\hat{V}(Q^2) = \hat{V}(0) \exp\left(-\frac{Q^2}{16\beta^2}\right), \tag{18}$$

inspired by the quark model [12] (as shown in Fig. 4). Finally, we get the result

TABLE III. The form factor $\hat{V}(Q^2)$ at different Q^2.

n	$Q^2(\mathrm{GeV}^2)$	$\hat{V}(Q^2)$
(0,2,2)	2.04	1.288(26)
(0,1,2)	1.29	1.499(10)
(0,0,2)	1.04	1.512(8)
(0,1,1)	0.52	1.784(10)
(0,0,1)	0.25	1.910(9)
...	0	2.083(11)

$$\hat{V}(0) = 2.083(11), \qquad \beta = 468(3)\ \mathrm{MeV}. \tag{19}$$

The value of fitted parameter $\hat{V}(0)$ is consistent with the previous lattice results, as listed in Table IV. By using the experimental values of $m_{J/\psi}$ and m_{η_c}, we predict the partial width $\Gamma(J/\psi \to \gamma\eta_c) = 2.77(3)$ keV, which is consistent with previous lattice results but is still larger than the PDG average $\Gamma(J/\psi \to \gamma\eta_c) = 1.57(37)$ keV [4].

B. $\chi_{c2} \to \gamma J/\psi$

The multipole decomposition of the transition amplitude for the decay $\chi_{c2} \to \gamma J/\psi$ is expressed as

$$\begin{aligned}&\langle J/\psi(\mathbf{p}_f, r_2)|J_\mu^{\mathrm{em}}(0)|\chi_{c2}(\mathbf{p}_i, r_1)\rangle \\ &= \alpha_\mu^1 E_1(Q^2) + \alpha_\mu^2 M_2(Q^2) + \alpha_\mu^3 E_3(Q^2) \\ &\quad + \alpha_\mu^4 C_1(Q^2) + \alpha_\mu^5 C_2(Q^2),\end{aligned} \tag{20}$$

where α_μ^k $(k = 1, 2, \ldots, 5)$ are Lorentz covariant kinematic functions of $p_{i,f}$ and polarization vectors of J/ψ and χ_{c2}, whose explicit expressions can be found in the Appendix and also in Refs. [14,16]. It should be noted that the $J = 2$ (for example, the spin of χ_{c2} and ψ_2) representation in the continuum breaks into E and T_2 irreducible representations of the octahedral group on a finite lattice. It is observed that this breaking effect is negligible as manifested by the nearly degenerate masses of tensor mesons derived from the E operator and T_2 operator. Subsequently, the multipole decomposition is performed on the basis of $E \oplus T_2$ [36].

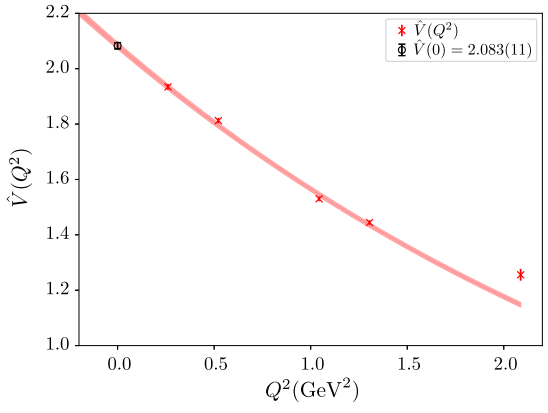

FIG. 4. The Q^2 extrapolation of $\hat{V}(Q^2)$. The shaded band shows the fit result using Eq. (18), and the black point is the value of $\hat{V}(Q^2 = 0)$ through the Q^2 extrapolation.

TABLE IV. The comparison of the form factor $\hat{V}(0)$ in this work with those in previous lattice QCD studies.

$\hat{V}(0)$	Reference
1.85(4)	[12]
2.01(2)	[15]
1.92(3)(2)	[37]
1.90(7)(1)	[18]
1.83–2.07	[27]
1.8649(73)	[38]
2.083(11)	This study

The decay width for $\chi_{c2} \to J/\psi\gamma$ involves only three on-shell form factors, namely, $E_1(0)$, $M_2(0)$, and $E_3(0)$, by the formula

$$\begin{aligned}\Gamma(\chi_{c2} \to \gamma J/\psi) = &\frac{16}{45}\alpha\frac{|q|}{m_{\chi_{c2}}^2} \\ &\times (|\hat{E}_1(0)|^2 + |\hat{M}_2(0)|^2 + |\hat{E}_3(0)|^2).\end{aligned} \tag{21}$$

So we focus on the extraction of these three form factors at different Q^2 and then perform the interpolation (extrapolation) to get the on-shell values. The procedure is very similar to that of $V(Q^2)$ for $J/\psi \to \gamma\eta_c$ except that t_f is $48a_t$ instead of $t_f = 64a_t$. (We also calculate the three-point function with $t_f = 64a_t$ and find the signals are very bad.) The t dependences of $\hat{E}_1(Q^2; t_f, t)$, $\hat{M}_2(Q^2; t_f, t)$, and $\hat{E}_3(Q^2; t_f, t)$ are shown in Fig. 5. By fitting these quantities using the function similar to Eq. (16), namely,

$$\begin{aligned}\hat{F}_k(Q^2, t) = &\hat{F}_k(Q^2)(1 + \delta_1^{(k)}(Q^2)e^{\Delta_1^{(k)}t} \\ &+ \delta_2^{(k)}(Q^2)e^{-\Delta_2^{(k)}(t_f - t)}),\end{aligned} \tag{22}$$

where $\hat{F}_k$ with $k = 1, 2, 3$ refer to $\hat{E}_1$, $\hat{M}_2$, and $\hat{E}_3$, respectively. The form factors $\hat{F}_k(Q^2)$ at different Q^2 are listed in Table V. For $\hat{E}_1(Q^2)$ and $\hat{M}_2(Q^2)$, the on-shell values $\hat{F}_k(Q^2 = 0)$ are interpolated through the function form

$$\hat{F}_k(Q^2) = \hat{F}_k(0)(1 + \lambda_k Q^2)\exp\left(-\frac{Q^2}{16\beta_k^2}\right). \tag{23}$$

Since the values of $\hat{E}_3(Q^2)$ are very small, we use a linear function $\hat{E}_3(Q^2) = \hat{E}_3(0) + aQ^2$ to perform the extrapolation. The fits for three form factors are illustrated in Fig. 6 by shaded bands. The extrapolated values of $\hat{F}_k(0)$ are also listed in Table V. The values of the on-shell form factors in

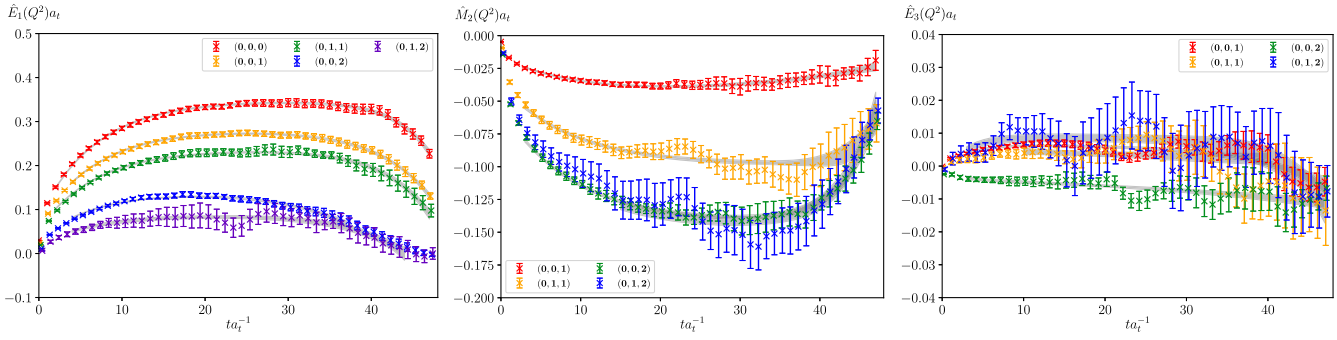

FIG. 5. Form factors $\hat{E}_1(Q^2)$, $\hat{M}_2(Q^2)$, and $\hat{E}_3(Q^2)$ versus ta_t^{-1} for the radiative transition $\chi_{c2} \to J/\psi\gamma$. The momentum of final particle is $\mathbf{p_f} = \frac{2\pi}{\mathbf{a_s L}}(\mathbf{n_x}\,\mathbf{n_y}\,\mathbf{n_z})$, and the legend denotes explicit values of (n_x, n_y, n_z). The points are lattice data, and the shaded bands are the fit results using the function form in Eq. (22).

TABLE V. The explicit value of the form factors $\hat{E}_1(Q^2)$, $\hat{M}_2(Q^2)$, and $\hat{E}_3(Q^2)$ for radiative transition $\chi_{c2} \to J/\psi\gamma$. The values are in physical units and are converted by $a_t^{-1} = 6.894(31)$ GeV.

n	Q^2 (GeV^2)	$\hat{E}_1(Q^2)$ (GeV)	$\hat{M}_2(Q^2)$ (GeV)	$\hat{E}_3(Q^2)$ (GeV)
(0,1,2)	1.21	0.609(28)	−1.006(31)	0.0608(92)
(0,0,2)	0.91	0.995(18)	−0.986(20)	−0.011(12)
(0,1,1)	0.33	1.634(14)	−0.679(14)	0.0321(51)
(0,0,1)	0.033	1.948(15)	−0.324(40)	0.0459(51)
(0,0,0)	−0.27	2.396(14)	⋯	⋯
⋯	0	2.025(13)	−0.267(38)	0.0362(42)

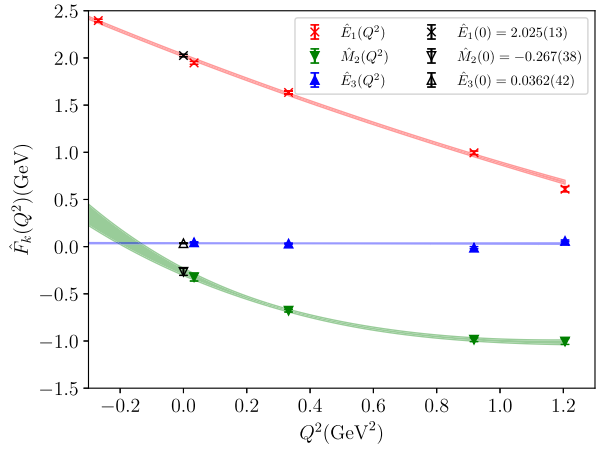

FIG. 6. The Q^2 interpolations or extrapolations of $\hat{E}_1(Q^2)$, $\hat{M}_2(Q^2)$, and $\hat{E}_3(Q^2)$ for $\chi_{c2} \to \gamma J/\psi$. $\hat{E}_1(Q^2)$, $\hat{M}_2(Q^2)$ are fitted using Eq. (23), while $\hat{E}_3(Q^2)$ is fitted using a linear equation in Q^2. The shaded bands illustrate the fit results, and the black points are the values at $Q^2 = 0$.

the last row of Table V indicate that the electric dipole (E_1) contribution dominates the decay process $\chi_{c2} \to \gamma J/\psi$, and the hierarchy $|E_1(0)| > |M_2(0)| \gg |E_3(0)|$ is described by the two ratios

$$a_2 = \frac{M_2(0)}{\sqrt{E_1(0)^2 + M_2(0)^2 + E_3(0)^2}} = -0.130(18),$$
$$a_3 = \frac{E_3(0)}{\sqrt{E_1(0)^2 + M_2(0)^2 + E_3(0)^2}} = 0.0177(21), \quad (24)$$

which are in agreement with the PDG values $a_2 = -0.11(1)$ and $a_3 = -0.003(10)$ [4].

With the interpolated values of $\hat{F}_k(0)$ and the experimental value of the masses of the mesons involved, the partial decay width of the decay χ_{c2} is predicted to be

$$\Gamma(\chi_{c2} \to \gamma J/\psi) = 368(5)\ \text{keV}, \quad (25)$$

which can be compared with the PDG average of 374 (10) keV [4] as well as the previous lattice results of 361 (9) keV [16] and 380(30) keV [14]. This comparison calibrates the uncontrolled systematic uncertainties of our calculation to some extent.

C. $\psi_2 \to \chi_{c1}\gamma$

The multipole decomposition of the transition matrix elements for $\psi_2 \to \gamma\chi_{c1}$ ($2^{--} \to 1^{++}$) is exactly the same as that for $\chi_{c2} \to \gamma J/\psi$ ($2^{++} \to 1^{--}$) [see Eq. (20)] [14,16]. The calculation of the related three-point function in Eq. (3) is performed in the rest frame of the initial state ψ_2. The subtlety in this case is that the generic quark bilinear operator $\mathcal{O}_{5i} \sim \bar{\psi}\gamma_5\gamma_i\psi$ for χ_{c1} couples both pseudoscalar mesons and axial vector mesons with the overlapping factors

$$\langle\Omega|\bar{\psi}\gamma_5\gamma_i\psi(0)|0^{-+}(\mathbf{p})\rangle = Z_P p_i,$$
$$\langle\Omega|\bar{\psi}\gamma_5\gamma_i\psi(0)|1^{++}(\mathbf{p},r)\rangle = Z_A\epsilon_i^{(r)}(\mathbf{p}), \quad (26)$$

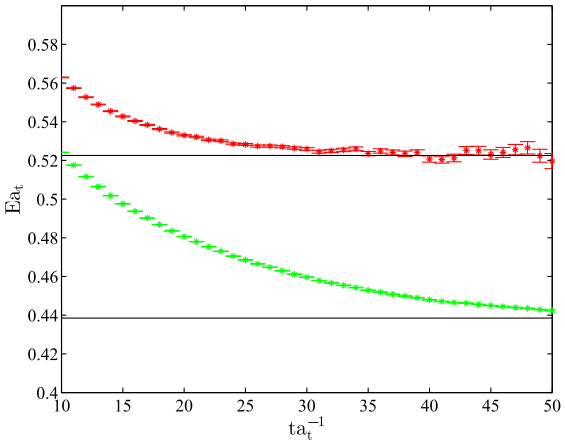

FIG. 7. The effective energies of the correlation functions of $\mathcal{O}_{5i}^{\mathbf{p}}(t)$ (green) and $\mathcal{O}_{5i}^{\mathrm{op}}(t,\mathbf{p})$ (red) for $\mathbf{p}$ mode $\mathbf{n}=(0,0,1)$. The black lines show the values of $E_{\eta_c}(\mathbf{p}a_t)$ and $E_{\chi_{c1}}(\mathbf{p})a_t$, respectively. Obviously, the optimized operator $\mathcal{O}_{5i}^{\mathrm{op}}(t,\mathbf{p})$ couples to χ_{c1} when t is large.

when the spatial momentum $\mathbf{p}$ is nonzero. Therefore, the contribution from pseudoscalar mesons (mainly η_c) should be eliminated when the three-point function $G_{f\mu i}(t_f,t;\mathbf{p}_f,\mathbf{p}_i)$ in Eq. (3) is computed. This is accomplished by choosing an optimized operator that couples predominantly to axial vector mesons. In doing so, for index i of $\mathcal{O}_{5i}$ and each momentum $\mathbf{p}$ with $p_i\neq 0$, we adopt the momentum projected operator $\mathcal{O}_5^{\mathbf{p}}$ to calculate the correlation matrix

$$\mathbf{C}(t)=\begin{pmatrix}\langle\Omega|\mathcal{O}_5^{\mathbf{p}}(t)\mathcal{O}_5^{\mathbf{p},\dagger}(0)|\Omega\rangle & \langle\Omega|\mathcal{O}_5^{\mathbf{p}}(t)\mathcal{O}_{5i}^{\mathbf{p},\dagger}(0)|\Omega\rangle\\ \langle\Omega|\mathcal{O}_{5i}^{\mathbf{p}}(t)\mathcal{O}_5^{\mathbf{p},\dagger}(0)|\Omega\rangle & \langle\Omega|\mathcal{O}_{5i}^{\mathbf{p}}(t)\mathcal{O}_{5i}^{\mathbf{p},\dagger}(0)|\Omega\rangle\end{pmatrix}. \tag{27}$$

Since $\mathcal{O}_5^{\mathbf{p}}$ couples exclusively to pseudoscalar mesons (η_c and its excited states), for properly chosen t and t_0, by solving the generalized eigenvalue problem $\mathbf{C}(t)\mathbf{v}=\lambda(t-t_0)\mathbf{C}(t_0)\mathbf{v}$ with $\mathbf{v}^T=(v_1,v_2)$ being an eigenvector, we can obtain the optimized operator that couples to axial vector mesons as follows:

$$\mathcal{O}_{5i}^{\mathrm{op}}(t,\mathbf{p})=v_1\,\mathcal{O}_5^{\mathbf{p}}(t)+v_2\mathcal{O}_{5i}^{\mathbf{p}}(t). \tag{28}$$

The effectiveness of this prescription is illustrated by Fig. 7, where the effective energies are plotted for the correlation function of $\mathcal{O}_{5i}$ (in green) and that of the optimized operator $\mathcal{O}_{5i}^{\mathrm{op}}$ (in red) for the momentum mode $\mathbf{n}=(0,0,1)$. It is seen that the effective energy of the former does not show a plateau but tends to the energy of η_c when t increases, while the effective energy of the latter reaches a plateau of a value consistent with the energy of χ_{c1} at this momentum. Therefore, for each momentum $\mathbf{p}$ mode of the final state χ_{c1}, we use the optimized operator $\mathcal{O}_{5i}^{\mathrm{op}}$ to calculate the three-point function $G_{f\mu i}$ in Eq. (3). The related transition matrix elements are extracted similarly to the cases of $J/\psi\to\gamma\eta_c$ and $\chi_{c2}\to\gamma J/\psi$ through Eq. (13).

The electromagnetic multipole decomposition of the matrix element is exactly the same as that for $\chi_{c2}\to\gamma J/\psi$ and is expressed in terms of five form factors $E_1(Q^2)$, $M_2(Q^2)$, $E_3(Q^2)$, $C_1(Q^2)$, and $C_2(Q^2)$. Considering that the final state photon is transversely polarized, only the former three form factors contribute to the partial width of the process $\psi_2\to\gamma\chi_{c2}$, namely,

$$\Gamma(\psi_2\to\gamma\chi_{c1})=\alpha\frac{16}{45}\frac{|\mathbf{q}|}{m_{\psi_2}^2}(|\hat{E}_1(0)|^2+|\hat{M}_2(0)|^2+|\hat{E}_3(0)|^2). \tag{29}$$

For different values of Q^2, the three form factors $\hat{E}_1(Q^2)$, $\hat{M}_2(Q^2)$, and $\hat{E}_3(Q^2)$ are extracted similarly to the case of $\chi_{c2}\to\gamma J/\psi$, as shown in Fig. 8, where the shaded bands illustrate the fit results using Eq. (16). The final values of form factors $\hat{E}_1(Q^2)$, $\hat{M}_2(Q^2)$, $\hat{E}_3(Q^2)$ are listed in Table VI along with the extrapolated values at $Q^2=0$

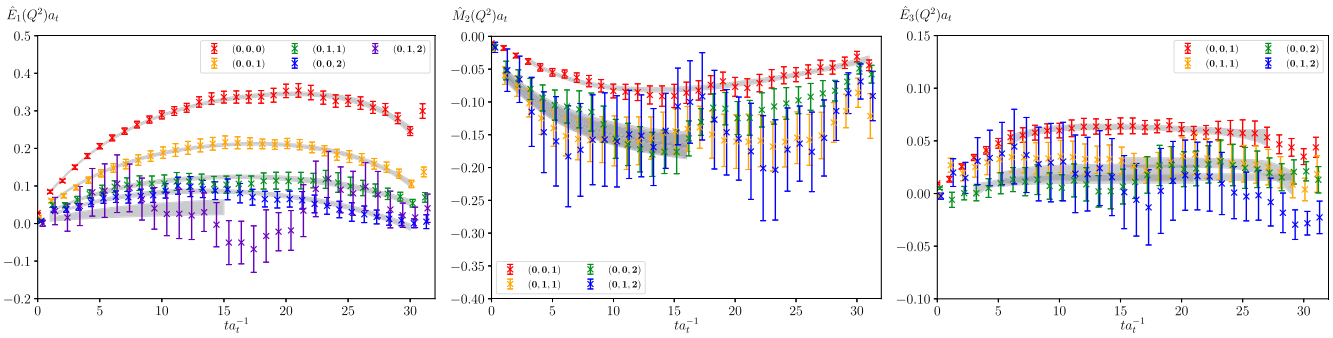

FIG. 8. Form factors $\hat{E}_1(Q^2)$, $\hat{M}_2(Q^2)$, and $\hat{E}_3(Q^2)$ versus ta_t^{-1} for the radiative transition $\psi_2\to\chi_{c1}\gamma$. The momentum of final particle is $\mathbf{p_f}=\frac{2\pi}{\mathbf{a_s L}}(\mathbf{n_x}\,\mathbf{n_y}\,\mathbf{n_z})$, and the legend denotes explicit values of (n_x,n_y,n_z). The points are lattice data, and the shaded bands are the fit results using the function form in Eq. (22).

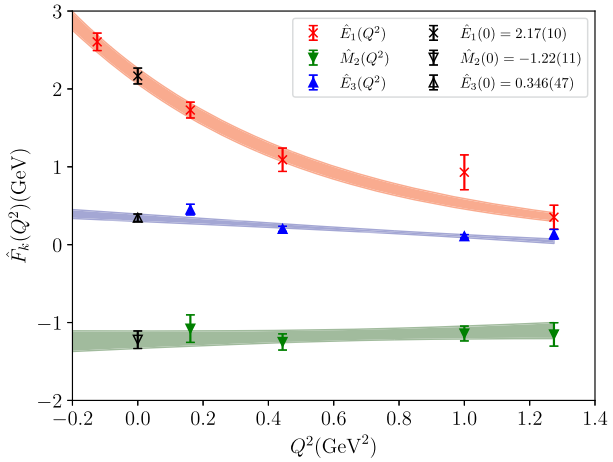

FIG. 9. The Q^2 interpolation or extrapolation of $\hat{E}_1(Q^2)$, $\hat{M}_2(Q^2)$, and $\hat{E}_3(Q^2)$ for $\psi_2 \to \gamma\chi_{c1}$. $\hat{E}_1(Q^2)$, $\hat{M}_2(Q^2)$ are fitted using Eq. (23), while $\hat{E}_3(Q^2)$ is fitted using a linear equation in Q^2. The shaded bands illustrate the fit results. and the black points are the values at $Q^2 = 0$.

using Eq. (23). The fits of form factors are illustrated in Fig. 9. After putting the values of $F_k(Q^2 = 0)$ into Eq. (29), the partial decay width of $\psi_2 \to \gamma\chi_{c1}$ is predicted to be

$$\Gamma(\psi_2 \to \gamma\chi_{c1}) = 337(27)\ \text{keV}. \tag{30}$$

It is seen that, although the dominant electric dipole (E_1) contribution is similar to the case of $\chi_{c2} \to \gamma J/\psi$, the contributions from the magnetic quadrupole (M_2) and the electric octupole (E_3) are substantial. Accordingly, we give the predictions

$$a_2 = \frac{M_2(0)}{\sqrt{E_1(0)^2 + M_2(0)^2 + E_3(0)^2}} = -0.485(37),$$
$$a_3 = \frac{E_3(0)}{\sqrt{E_1(0)^2 + M_2(0)^2 + E_3(0)^2}} = 0.137(19). \tag{31}$$

TABLE VI. The explicit values of form factors $\hat{E}_1(Q^2)$, $\hat{M}_2(Q^2)$, and $\hat{E}_3(Q^2)$ for radiative transition $\psi_2 \to \chi_{c1}\gamma$.

n	Q^2 (GeV^2)	$\hat{E}_1(Q^2)$ (GeV)	$\hat{M}_2(Q^2)$ (GeV)	$\hat{E}_3(Q^2)$ (GeV)
(0,1,2)	1.27	0.35(15)	–1.15(15)	0.133(62)
(0,0,2)	1.00	0.92(22)	–1.140(95)	0.108(22)
(0,1,1)	0.44	1.09(15)	–1.24(10)	0.203(33)
(0,0,1)	0.16	1.72(10)	–1.07(18)	0.451(69)
(0,0,0)	–0.12	2.60(11)		
…	0	2.17(10)	–1.22(11)	0.346(47)

D. Discussion

As has been shown in the previous sections, the obtained form factors for transitions $J/\psi \to \gamma\eta_c$ and $\chi_{c2} \to \gamma J/\psi$ based on our lattice setup are consistent with previous lattice results. Especially, our prediction for the partial width and the hierarchy of $|E_1(0)| > |M_2(0)| \gg |E_3(0)|$ of the process $\chi_{c2} \to \gamma J/\psi$ are in quantitatively agreement with the experimental data. This comparison justifies the reliability of our predictions for the process $\psi_2 \to \gamma\chi_{c1}$.

There have been quite a lot of phenomenological studies on radiative charmonium transitions using various theoretical frameworks, such as the nonrelativistic QCD approach (NRQCD), the nonrelativistic quark models (QM) with different confining potentials, the relativistic quark models, the Bethe-Salpeter wave function method, etc. Their predictions for the partial decay widths of $\chi_{c2} \to \gamma J/\psi$ and $\psi_2 \to \gamma\chi_{c1}$ are collected in Table VII along with the precise references. Also shown are the previous lattice QCD predictions in the quenched approximation (QLQCD), the experimental values, and the results in this work.

TABLE VII. Comparison of the predictions of $\Gamma(\chi_{c2} \to \gamma J/\psi)$ and $\Gamma(\psi_2 \to \gamma\chi_{c1})$ by different theoretical formalism. The abbreviations in the most right column refer to the nonrelativistic QCD approach (NRQCD), the nonrelativistic quark models (QM), the relativistic quark models (RQM), the Bethe-Salpeter equation (BS), and the quenched lattice QCD (QLQCD) calculations, respectively. Various confining potentials are adopted in QM and RQM approaches, and the details can be found in the corresponding references. The experimental value and the predictions of this work are shown in bold numbers.

$\Gamma(\chi_{c2} \to \gamma J/\psi)$ (keV)	$\Gamma(\psi_2 \to \gamma\chi_{c1})$ (keV)	Formalism
282 [39]	250 [40]	NRQCD
401 [39]	…	NRQCD
315	260	QM [41]
424	307	QM [8]
473	342	QM [42]
309	208	QM [42]
327	281	QM [43]
338	291	QM [43]
313	268	RQM [8]
448	297	RQM [7]
309	215	RQM [7]
292	215	RQM [7]
327	215	RQM [7]
…	265	BS [44]
361(9)	…	QLQCD [16]
380(50)	…	QLQCD [14]
368(5)	337(27)	This work
374(10)	…	PDG2022 [4]

As far as the $\chi_{c2} \to \gamma J/\psi$ transition is concerned, the phenomenological predictions of the partial width range from 280 to 450 keV and are consistent with the experimental value 374(10) keV when considering the theoretical uncertainties owing to the model assumptions. The values by QLQCD are more converged and agree quantitatively with the PDG value. Our result $\Gamma(\chi_{c2} \to \gamma J/\psi) = 368(5)$ keV is the first prediction from the lattice QCD with light dynamical quarks and is in excellent agreement with QLQCD results and the PDG value.

We also give the first lattice QCD prediction $\Gamma(\psi_2 \to \gamma\chi_{c2}) = 337(27)$ keV, whose central value is slightly larger than the phenomenological predictions (see Table VII), most of which are below 300 keV. On the other hand, BESIII measured the branching-fraction ratios $\mathcal{B}(\psi_2(3823) \to X)/\mathcal{B}(\psi_2(3823) \to \gamma\chi_{c1})$ with X referring to the decay channels $\gamma\chi_{c2}$, $\pi^+\pi^- J/\psi$, $\pi^0\pi^0 J/\psi$, $\eta J/\psi$, $\pi^0 J/\psi$, and $\gamma\chi_{c0}$ [3], which are quoted in Table VIII. These ratios are equivalently the ratios of the corresponding partial decay widths $\Gamma(\psi_2(3823) \to X)/\Gamma(\psi_2(3823) \to \gamma\chi_{c1})$. Based on these results, we can estimate the total width of ψ_2 as follows:

(i) $\Gamma(\psi_2(3823) \to \gamma\chi_{c2})$: According to the branching-fraction ratio measured by BESIII, this partial width is estimated to be 94^{+49}_{-39} keV.

(ii) $\Gamma(\psi_2(3823) \to \pi\pi J/\psi)$: Although BESIII gives individual upper limits for the branching-fraction ratios 0.06 and 0.11 for $\pi^+\pi^- J/\psi$ and $\pi^0\pi^0 J/\psi$ decay channels, respectively, the isospin symmetry implies that $\Gamma(\pi^+\pi^- J/\psi)/\Gamma(\pi^0\pi^0 J/\psi) \approx 2$. Therefore, we assume $\Gamma(\psi_2(3823) \to \pi\pi J/\psi)/\Gamma(\psi_2(3823) \to \gamma\chi_{c1}) < 0.1$, which implies $\Gamma(\psi_2(3823) \to \pi\pi J/\psi) < 34(3)$ keV. This is compatible with the QM prediction $\Gamma(\psi_2(3823) \to \pi\pi J/\psi) \approx 45$ keV [41], but much smaller than the value of 160 keV predicted by Ref. [9].

(iii) $\Gamma(\psi_2(3823) \to \eta J/\psi)$: The flavor SU(3) symmetry requires the η in the final state is produced through gluons coupling to its flavor singlet component. The small $\eta - \eta'$ mixing angle θ (the partial width is proportional to $\sin^2\theta$) and the centrifugal barrier (η and J/ψ are in P wave) suppresses the decay rate of this process, but the QCD $U_A(1)$ anomaly enhances the coupling of gluons to η and may counteract the suppression. Referring to the branching-fraction ratio $\frac{\mathcal{B}(\psi(3770)\to\pi\pi J/\psi)}{\mathcal{B}(\psi(3770)\to\eta J/\psi)} \approx 3$ [4], $\Gamma(\psi_2(3823) \to \eta J/\psi) < 20$ keV might be a reasonable estimate even though BESIII gives a higher upper limit.

(iv) $\Gamma(\psi_2(3823) \to \gamma\chi_{c0}, \gamma\eta_c)$: These two partial widths are predicted to be ~1 keV by a phenomenological study through the Bethe-Salpeter equation approach [44].

(v) $\Gamma(\psi_2(3823) \to \pi^0 J/\psi)$: The partial width of this isospin breaking decay channel can be neglected.

(vi) $\Gamma(\psi_2(3823) \to$ light hadrons): The total decay widths of $\psi_2(3823) \to$ light hadrons can be approximated by $\Gamma(\psi_2 \to ggg) \sim 36$ keV [41].

Summing over all the contributions mentioned above, we can give a raw estimate of the total width of $\psi_2(3823)$,

$$\Gamma(\psi_2(3823)) \approx 520 \pm 100 \text{ keV}, \tag{32}$$

where the uncertainty mainly comes from the partial widths of $\psi_2(3823) \to \gamma\chi_{c1}, \chi_{c2}$ and can be reduced by a refined lattice QCD calculation of $\Gamma(\psi_2(3823) \to \gamma\chi_{c1})$ and a direct lattice calculation of $\Gamma(\psi_2(3823) \to \gamma\chi_{c2})$ in the future.

TABLE VIII. The branching-fraction ratios $\frac{\mathcal{B}(\psi_2(3823)\to X)}{\mathcal{B}(\psi_2(3823)\to\gamma\chi_{c1})}$ measured by BESIII [3] with X referring to the decay channels $\gamma\chi_{c2}$, $\pi^+\pi^- J/\psi$, $\pi^0\pi^0 J/\psi$, $\eta J/\psi$, $\pi^0 J/\psi$ and $\gamma\chi_{c0}$.

Channel (X)	$\frac{\mathcal{B}(\psi_2(3823)\to X)}{\mathcal{B}(\psi_2(3823)\to\gamma\chi_{c1})}$
$\gamma\chi_{c2}$	$0.28^{+0.14}_{-0.11} \pm 0.02$
$\pi^+\pi^- J/\psi$	<0.06
$\pi^0\pi^0 J/\psi$	<0.11
$\eta J/\psi$	<0.14
$\pi^0 J/\psi$	<0.03
$\gamma\chi_{c0}$	<0.24

V. SUMMARY

We perform an exploratory $N_f = 2$ lattice QCD study on the radiative transition $\psi_2(3823) \to \gamma\chi_{c1}$ in the framework of the distillation method. On a single gauge ensemble with a pion mass $m_\pi \sim 350$ MeV, the electromagnetic multipole form factors are extracted for the processes $J/\psi \to \gamma\eta_c$, $\chi_{c2} \to \gamma J/\psi$ and $\psi_2 \to \gamma\chi_{c1}$. The obtained $\hat{V}(0) = 2.083(11)$ for $J/\psi \to \gamma\eta_c$ is consistent with previous lattice results, but the result $\Gamma(J/\psi \to \gamma\eta_c) = 2.77(3)$ keV is still larger than the PDG average. For $\chi_{c2} \to \gamma J/\psi$, we extract the on-shell form factors $E_1(0)$, $M_2(0)$, and $E_3(0)$, whose hierarchy $|E_1(0)| > |M_2(0)| \gg |E_3(0)|$ is in quantitative agreement with the experimental results. We predict $\Gamma(\chi_{c2} \to \gamma J/\psi) = 368(5)$ keV, which is in excellent agreement with the PDG value 374(10) keV and previous QLQCD results. This is the first result from lattice QCD with dynamical light quarks. No quenched effects are observed here.

We present the first lattice QCD prediction of the partial decay width $\Gamma(\psi_2(3823) \to \gamma\chi_{c1}) = 337(27)$ keV, whose central value is higher than most of the phenomenological results. According to the BESIII measurement of branching fractions of $\psi_2(3823)$ decay channels and some phenomenological results, we estimate the total width $\Gamma(\psi_2(3823)) = 520(100)$ keV. A direct lattice QCD calculation of the partial widths of $\psi_2 \to \gamma\chi_{c2}, \gamma\chi_{c0}, \gamma\eta_c$ will

reduce the uncertainty of the total width. This can be fulfilled in the future.

ACKNOWLEDGMENTS

This work is supported in part by the National Natural Science Foundation of China (NNSFC) under Grants No. 12075176, No. 11935017, No. 12293060, No. 12293065, and No. 12070131001 (CRC 110 by DFG and NNSFC), the Innovation Capability Support Program of Shaanxi (Program No. 2022KJXX-42), and 2022 Shaanxi University Youth Innovation Team Project (K20220186). Y. C. also acknowledges the support by the National Key Research and Development Program of China (Grant No. 2020YFA0406400) and the Strategic Priority Research Program of Chinese Academy of Sciences (Grant No. XDB34030302). The Chroma software system [45] and QUDA library [46,47] are acknowledged. The simulations were performed on the HPC clusters at Institute of High Energy Physics (Beijing) and China Spallation Neutron Source (Dongguan).

APPENDIX: MULTIPOLE DECOMOPOSITION OF $\langle V|j^\mu|T\rangle$

Generally speaking, the radiative transition amplitude of the process $(J\lambda) \to (J'\lambda') + \gamma(\lambda_\gamma)$,

$$\mathcal{M}(\lambda_\gamma) \equiv \langle J'\lambda'|J^{\rm em}_\mu(0)|J\lambda\rangle \epsilon^*_\mu(\lambda_\gamma), \tag{A1}$$

can be expressed in terms of the electromagnetic multipole form factors E_k, M_k and C_k as [14,16]

$$\begin{aligned}
\mathcal{M}(\lambda_\gamma = \pm) &= \sum_k \sqrt{\frac{2k+1}{2J+1}} \left[E_k \frac{1}{2}(1 + (-)^k \delta P) \mp M_k \frac{1}{2}(1 - (-)^k \delta P) \right] \langle k\pm; J'\lambda \pm 1|J\lambda\rangle, \\
\mathcal{M}(\lambda_\gamma = 0) &= \sum_k \sqrt{\frac{2k+1}{2J+1}} C_k \frac{1}{2}(1 + (-)^k \delta P) \langle k0; J'\lambda'|J\lambda\rangle,
\end{aligned} \tag{A2}$$

where $J(J')$ and $\lambda(\lambda')$ are the spin and the helicity of the initial(final) state meson, respectively, and δP is the product of the parities of the initial and final states. Note that the number of form factors are determined by the Clebsch-Gordan coefficients $\langle k\lambda_\gamma; J'\lambda'|J\lambda\rangle$ for given J and J'. Constrained to the case of the initial $J^P = 2^\pm$ meson (T) and the final $J^P = 1^\mp$ meson (V) in this study, it is easy to see that only the form factors E_1, M_2, and E_3 are involved in the partial decay width.

On the other hand, the Lorentz structure of the transition matrix of $T \to V + \gamma$ can be written as

$$\langle V(\mathbf{p}_f, r_2)|J^{\rm em}_\mu(0)|T(\mathbf{p}_i, r_1)\rangle = a(Q^2)A_\mu + b(Q^2)B_\mu + c(Q^2)C_\mu + d_T(Q^2)D^T_\mu + d_V(Q^2)D^V_\mu + f_V(Q^2)F^V_\mu, \tag{A3}$$

with the definitions

$$\begin{aligned}
&A_\mu \equiv \epsilon_{\mu\nu}(\mathbf{p}_i, r_1)\epsilon^{*\nu}(\mathbf{p}_f, r_2), \qquad B_\mu \equiv \epsilon_{\mu\nu}(\mathbf{p}_i, r_1)p^\nu_f(\epsilon^*(\mathbf{p}_f, r_2)\cdot p_i), \qquad C_\mu \equiv \epsilon^*_\mu(\mathbf{p}_f, r_2)(\epsilon_{\alpha\beta}(\mathbf{p}_i, r_1)p^\alpha_f p^\beta_f), \\
&D^T_\mu \equiv p_{i,\mu}(\epsilon_{\alpha\beta}\epsilon^{*,\alpha}(\mathbf{p}_f, r_2)p^\beta_f), \qquad D^V_\mu \equiv p_{f,\mu}(\epsilon_{\alpha\beta}(\mathbf{p}_i, r_1)\epsilon^{*,\alpha}(\mathbf{p}_f, r_2)p^\beta_f), \\
&F^T_\mu \equiv p_{i,\mu}(\epsilon_{\alpha\beta}(\mathbf{p}_i, r_1)p^\alpha_f p^\beta_f)(\epsilon^*(\mathbf{p}_f, r_2)\cdot p_i), \qquad F^V_\mu \equiv p_{f,\mu}(\epsilon_{\alpha\beta}(\mathbf{p}_i, r_1)p^\alpha_f p^\beta_f)(\epsilon^*(\mathbf{p}_f, r_2)\cdot p_i).
\end{aligned} \tag{A4}$$

Here, the C and P parity conservation is assumed implicitly. In the practical calculation of this work, the polarization vectors $\epsilon_{\mu\nu}(p_i, r_1)$ of the tensor state T in the above equations are expressed on the basis of $E \otimes T_2$, since E and T_2 are the subduced irreducible representation of the $J = 2$ representation of the rotational group SO(3) onto the lattice symmetry group, namely, the octahedral group O. Although E and T_2 are different representations for a finite lattice spacing, their differences are tested to be negligible in our lattice setup. Along with the Ward identity,

$$\partial^\mu \langle V(p_f)|J^{\rm em}_\mu(x)|T(p_i)\rangle \equiv -i(p_i - p_f)^\mu \langle V(p_f)|J^{\rm em}_\mu(x)|T(p_i)\rangle \equiv 0, \tag{A5}$$

and combining Eqs. (A1)–(A4), after some calculus one obtains

$$\langle V(\mathbf{p}_f, r_2)|J^{\rm em}_\mu(0)|T(\mathbf{p}_i, r_1)\rangle = \alpha^1_\mu E_1(Q^2) + \alpha^2_\mu M_2(Q^2) + \alpha^3_\mu E_3(Q^2) + \alpha^4_\mu C_1(Q^2) + \alpha^5_\mu C_3(Q^2), \tag{A6}$$

where $Q^2 = -(p_f - p_i)^2 \equiv -q^2$ is defined, and the explicit expressions of α_μ^i are as follows [14,16]:

$$\alpha_\mu^1 = \sqrt{\frac{3}{5}}\left[-A_\mu + \frac{m_i}{\Omega}(\omega - m_f)B_\mu + \frac{m_i}{\Omega}(\omega D_\mu^T - m_i D_\mu^V) + \frac{m_i^2}{\Omega^2}(\omega - m_f)(-\omega F_\mu^T + m_i F_\mu^V)\right],$$

$$\alpha_\mu^2 = \sqrt{\frac{1}{3}}\left[A_\mu - \frac{m_i}{\Omega}(\omega + m_f)B_\mu - \frac{2m_i^2}{\Omega}C_\mu - \frac{m_i}{\Omega}(\omega D_\mu^T - m_i D_\mu^V) + \frac{m_i^2}{\Omega^2}((\omega^2 + \omega m_f - 2m_f^2)F_\mu^T + m_i(\omega - m_f)F_\mu^V)\right],$$

$$\alpha_\mu^3 = \sqrt{\frac{1}{15}}\left[-A_\mu + m_i/\Omega(\omega + 4m_f)B_\mu - \frac{5m_i^2}{2\Omega}C_\mu + \frac{m_i}{\Omega}(\omega D_\mu^T - m_i D_\mu^V) + \frac{m_i^2}{\Omega^2}\left(-\left(\omega^2 + 4\omega m_f + \frac{5}{2}m_f^2\right)F_\mu^T + m_i\left(\frac{7}{2}\omega + 4m_f\right)F_\mu^V\right)\right],$$

$$\alpha_\mu^4 = \sqrt{\frac{3}{5}}\frac{m_i}{\Omega\sqrt{q^2}}\left[(m_f^2 - \omega m_i)D_\mu^T + (m_i^2 - \omega m_i)D_\mu^V - \frac{m_i}{\Omega}(\omega - m_f)((m_f^2 - \omega m_i)F_\mu^T + (m_i^2 - \omega m_i)F_\mu^V)\right],$$

$$\alpha_\mu^5 = \sqrt{\frac{2}{5}}\frac{m_i}{\Omega\sqrt{q^2}}\left[(m_f^2 - \omega m_i)D_\mu^T + (m_i^2 - \omega m_i)D_\mu^V - \frac{m_i}{\Omega}\left(\omega + \frac{3}{2}m_f\right)((m_f^2 - \omega m_i)F_\mu^T + (m_i^2 - \omega m_i)F_\mu^V)\right]. \tag{A7}$$

In the expressions above, we introduce two Lorentz invariant quantities,

$$\Omega \equiv (p_i \cdot p_f)^2 - m_i^2 m_f^2, \qquad \omega = \frac{p_i \cdot p_f}{m_i}. \tag{A8}$$

[1] V. Bhardwaj *et al.* (Belle Collaboration), Evidence of a new narrow resonance decaying to $\chi_{c1}\gamma$ in $B \to \chi_{c1}\gamma K$, Phys. Rev. Lett. **111**, 032001 (2013).

[2] M. Ablikim *et al.* (BESIII Collaboration), Observation of the $\psi(1^3D_2)$ state in $e^+e^- \to \pi^+\pi^-\gamma\chi_{c1}$ at BESIII, Phys. Rev. Lett. **115**, 011803 (2015).

[3] M. Ablikim *et al.* (BESIII Collaboration), Search for new decay modes of the $\psi_2(3823)$ and the process $e^+e^- \to \pi^0\pi^0\psi_2(3823)$, Phys. Rev. D **103**, L091102 (2021).

[4] R. L. Workman *et al.* (Particle Data Group), Review of particle physics, Prog. Theor. Exp. Phys. **2022**, 083C01 (2022).

[5] M. Ablikim *et al.* (BESIII Collaboration), Observation of $e^+e^- \to \pi^0\pi^0\psi_2(3823)$, J. High Energy Phys. 02 (2023) 171.

[6] R. Aaij *et al.* (LHCb Collaboration), Near-threshold $D\overline{D}$ spectroscopy and observation of a new charmonium state, J. High Energy Phys. 07 (2019) 035.

[7] D. Ebert, R. N. Faustov, and V. O. Galkin, Properties of heavy quarkonia and B_c mesons in the relativistic quark model, Phys. Rev. D **67**, 014027 (2003).

[8] T. Barnes, S. Godfrey, and E. S. Swanson, Higher charmonia, Phys. Rev. D **72**, 054026 (2005).

[9] B. Wang, H. Xu, X. Liu, D.-Y. Chen, S. Coito, and E. Eichten, Using $X(3823) \to J/\psi\pi^+\pi^-$ to identify coupled-channel effects, Front. Phys. (Beijing) **11**, 111402 (2016).

[10] R. Aaij *et al.* (LHCb Collaboration), Study of the $\psi_2(3823)$ and $\chi_{c1}(3872)$ states in $B^+ \to (J/\psi\pi^+\pi^-)K^+$ decays, J. High Energy Phys. 08 (2020) 123.

[11] M. Ablikim *et al.* (BESIII Collaboration), Observation of resonance structures in $e^+e^- \to \pi^+\pi^-\psi_2(3823)$ and mass measurement of $\psi_2(3823)$, Phys. Rev. Lett. **129**, 102003 (2022).

[12] J. J. Dudek, R. G. Edwards, and D. G. Richards, Radiative transitions in charmonium from lattice QCD, Phys. Rev. D **73**, 074507 (2006).

[13] J. J. Dudek and R. G. Edwards, Two photon decays of charmonia from lattice QCD, Phys. Rev. Lett. **97**, 172001 (2006).

[14] J. J. Dudek, R. Edwards, and C. E. Thomas, Exotic and excited-state radiative transitions in charmonium from lattice QCD, Phys. Rev. D **79**, 094504 (2009).

[15] Y. Chen *et al.*, Radiative transitions in charmonium from $N_f = 2$ twisted mass lattice QCD, Phys. Rev. D **84**, 034503 (2011).

[16] Y.-B. Yang, Y. Chen, L.-C. Gui, C. Liu, Y.-B. Liu, Z. Liu, J.-P. Ma, and J.-B. Zhang (CLQCD Collaboration), Lattice study on η_{c2} and X(3872), Phys. Rev. D **87**, 014501 (2013).

[17] L.-C. Gui, Y. Chen, G. Li, C. Liu, Y.-B. Liu, J.-P. Ma, Y.-B. Yang, and J.-B. Zhang (CLQCD Collaboration), Scalar glueball in radiative J/ψ decay on the lattice, Phys. Rev. Lett. **110**, 021601 (2013).

[18] G. C. Donald, C. T. H. Davies, R. J. Dowdall, E. Follana, K. Hornbostel, J. Koponen, G. P. Lepage, and C. McNeile, Precision tests of the J/ψ from full lattice QCD: Mass, leptonic width and radiative decay rate to η_c, Phys. Rev. D **86**, 094501 (2012).

[19] Y.-B. Yang, L.-C. Gui, Y. Chen, C. Liu, Y.-B. Liu, J.-P. Ma, and J.-B. Zhang (CLQCD Collaboration), Lattice study of radiative J/ψ decay to a tensor glueball, Phys. Rev. Lett. **111**, 091601 (2013).

[20] D. Bečirević, M. Kruse, and F. Sanfilippo, Lattice QCD estimate of the $\eta_c(2S) \to J/\psi\gamma$ decay rate, J. High Energy Phys. 05 (2015) 014.

[21] L.-C. Gui, J.-M. Dong, Y. Chen, and Y.-B. Yang, Study of the pseudoscalar glueball in J/ψ radiative decays, Phys. Rev. D **100**, 054511 (2019).

[22] Y. Meng, C. Liu, and K.-L. Zhang, Three photon decay of J/ψ from lattice QCD, Phys. Rev. D **102**, 054506 (2020).

[23] C. Liu, Y. Meng, and K.-L. Zhang, Ward identity of the vector current and the decay rate of $\eta_c \to \gamma\gamma$ in lattice QCD, Phys. Rev. D **102**, 034502 (2020).

[24] N. Li, C.-C. Liu, and Y.-J. Wu, Radiative transition for $X_{c0} \to J/\psi\gamma$ from $N_f = 2$ twisted mass lattice QCD, Europhys. Lett. **133**, 11001 (2021).

[25] X. Jiang, F. Chen, Y. Chen, M. Gong, N. Li, Z. Liu, W. Sun, and R. Zhang, Radiative decay width of $J/\psi \to \gamma\eta_{(2)}$ from $N_f = 2$ lattice QCD, Phys. Rev. Lett. **130**, 061901 (2023).

[26] F. Chen, X. Jiang, Y. Chen, M. Gong, Z. Liu, C. Shi, and W. Sun, 1^{-+} hybrid meson in J/ψ radiative decays from lattice QCD, Phys. Rev. D **107**, 054511 (2023).

[27] J. Delaney, C. E. Thomas, and S. M. Ryan, Radiative transitions in charmonium from lattice QCD, arXiv:2301.08213.

[28] B. Colquhoun, L. Cooper, C. Davies, and G. P. Lepage, Precise determination of decay rates for $\eta_c \to \gamma\gamma$ and $J/\psi \to \gamma\eta_c$, Proc. Sci. LATTICE2022 (**2023**) 054.

[29] M. Peardon, J. Bulava, J. Foley, C. Morningstar, J. Dudek, R. G. Edwards, B. Joo, H.-W. Lin, D. G. Richards, and K. J. Juge (Hadron Spectrum Collaboration), A Novel quark-field creation operator construction for hadronic physics in lattice QCD, Phys. Rev. D **80**, 054506 (2009).

[30] C. J. Shultz, J. J. Dudek, and R. G. Edwards, Excited meson radiative transitions from lattice QCD using variationally optimized operators, Phys. Rev. D **91**, 114501 (2015).

[31] X. Jiang, W. Sun, F. Chen, Y. Chen, M. Gong, Z. Liu, and R. Zhang, η-glueball mixing from $N_f = 2$ lattice QCD, Phys. Rev. D **107**, 094510 (2023).

[32] J.-h. Zhang and C. Liu, Tuning the tadpole improved clover Wilson action on coarse anisotropic lattices, Mod. Phys. Lett. A **16**, 1841 (2001).

[33] S.-q. Su, L.-m. Liu, X. Li, and C. Liu, A Numerical study of improved quark actions on anisotropic lattices, Int. J. Mod. Phys. A **21**, 1015 (2006).

[34] G.-Z. Meng *et al.* (CLQCD Collaboration), Low-energy $D^{*+}\bar{D}_1^0$ scattering and the resonance-like structure $Z^+(4430)$, Phys. Rev. D **80**, 034503 (2009).

[35] R. Zhang, W. Sun, F. Chen, Y. Chen, M. Gong, X. Jiang, and Z. Liu, Annihilation diagram contribution to charmonium masses, Chin. Phys. C **46**, 043102 (2022).

[36] J. J. Dudek, R. G. Edwards, N. Mathur, and D. G. Richards, Charmonium excited state spectrum in lattice QCD, Phys. Rev. D **77**, 034501 (2008).

[37] D. Becirevic and F. Sanfilippo, Lattice QCD study of the radiative decays $J/\psi \to \eta_c\gamma$ and $h_c \to \eta_c\gamma$, J. High Energy Phys. 01 (2013) 028.

[38] B. Colquhoun, L. J. Cooper, C. T. H. Davies, and G. P. Lepage, Precise determination of decay rates for $\eta_c \to \gamma\gamma$, $J/\psi \to \gamma\eta_c$ and $J/\psi \to \eta_c e^+e^-$ from lattice QCD, Phys. Rev. D **108**, 014513 (2023).

[39] K.-T. Chao, Y.-B. Ding, and D.-H. Qin, Some problems on the charmonium p wave singlet state, Phys. Lett. B **301**, 282 (1993).

[40] C.-f. Qiao, F. Yuan, and K.-T. Chao, A crucial test for color octet production mechanism in Z^0 decays, Phys. Rev. D **55**, 4001 (1997).

[41] E. J. Eichten, K. Lane, and C. Quigg, B meson gateways to missing charmonium levels, Phys. Rev. Lett. **89**, 162002 (2002).

[42] B.-Q. Li and K.-T. Chao, Higher charmonia and X,Y,Z states with screened potential, Phys. Rev. D **79**, 094004 (2009).

[43] W.-J. Deng, H. Liu, L.-C. Gui, and X.-H. Zhong, Charmonium spectrum and their electromagnetic transitions with higher multipole contributions, Phys. Rev. D **95**, 034026 (2017).

[44] W. Li, S.-Y. Pei, T. Wang, Y.-L. Wang, T.-F. Feng, and G.-L. Wang, Electromagnetic decays of $X(3823)$ as the $\psi_2(1^3D_2)$ state and its radial excited states, Phys. Rev. D **107**, 113002 (2023).

[45] R. G. Edwards and B. Joo (SciDAC, LHPC, UKQCD Collaborations), The Chroma software system for lattice QCD, Nucl. Phys. B, Proc. Suppl. **140**, 832 (2005).

[46] M. A. Clark, R. Babich, K. Barros, R. C. Brower, and C. Rebbi, Solving Lattice QCD systems of equations using mixed precision solvers on GPUs, Comput. Phys. Commun. **181**, 1517 (2010).

[47] R. Babich, M. A. Clark, B. Joo, G. Shi, R. C. Brower, and S. Gottlieb, Scaling lattice QCD beyond 100 GPUs, in *SC11 International Conference for High Performance Computing, Networking, Storage and Analysis* (2011), arXiv:1109.2935.